Materials Transactions, Vol. 43, No. 4 (2002) pp. 660 to 666

Effects of Metastable Phase Formation on the Magnetic Properties of $Pr_{4.5}Fe_{77}B_{18.5}$ Amorphous Ribbons

Yun-Chul Jung[1], Yasuya Ohmori[1], Kiyomichi Nakai[1], Satoshi Hirosawa[2] and Hirokazu Kanekiyo[2]

[1]*Department of Materials Science and Engineering, Faculty of Engineering, Ehime University, Matsuyama 790-8577, Japan*
[2]*Research and Development Division, Sumitomo Special Metals Co. Ltd., Shimamoto-cho, Osaka 618-0013, Japan*

The effects of isothermal annealing on the magnetic properties of $Pr_{4.5}Fe_{77}B_{18.5}$ amorphous ribbons have been investigated. Two separate reactions increasing coercive force (H_c) were recognized during the progress of annealing. In the first reaction, hard magnetic $Pr_2Fe_{14}B$ particles with nanoscale diameters precipitated in the vicinity of Fe_3B and $Pr_2Fe_{23}B_3$ particles. The precipitation of fine $Pr_2Fe_{14}B$ particles increased H_c largely but reduced saturation magnetization (M_s) significantly. In the second reaction, the $Pr_2Fe_{23}B_3$ particles decomposed into $Pr_2Fe_{14}B$ particles containing very fine α-Fe particles within them. This resulted in the second increase in H_c due to both the volume fraction increase of $Pr_2Fe_{14}B$ particles and the exchange-coupling interaction between the $Pr_2Fe_{14}B$ grains and α-Fe particles within them. This phenomenon was observed originally in the present study. In the final stages of annealing, both H_c and M_s were decreased substantially by the decomposition of $Pr_2Fe_{14}B$ into $PrFe_4B_4$ particle in addition to the coarsening of α-Fe particles.

(Received October 29, 2001; Accepted February 6, 2002)

Keywords: *praseodymium-iron-boron amorphous ribbon, isothermal annealing, crystallization, phase decomposition, metastable phase, magnetic property*

1. Introduction

The hard magnetic properties of rare earth (RE)-Fe–B amorphous ribbons with low RE contents are largely improved by the crystallization of amorphous phase at temperatures from 600 to 800°C.[1–10] The alloys showing such hard magnetic properties are composed of large amounts of soft magnetic particles such as Fe_3B, $RE_2Fe_{23}B_3$ and α-Fe and small amounts of hard magnetic $RE_2Fe_{14}B$ particles exhibiting large magnetocrystalline anisotropy.[9,11,12] The magnetic properties of these alloys depend on the phases precipitated, the grain size, the distribution and the interphase boundary structures between hard and soft magnetic particles.[13–16]

In the previous study on a $Pr_{4.5}Fe_{77}B_{18.5}$ amorphous ribbon,[17] it has been confirmed that the precipitation sequence during isothermal annealing is; amorphous (Am) $\rightarrow$ Fe_3B + [Am] $\rightarrow$ $Pr_2Fe_{23}B_3$ + [Am + Fe_3B] $\rightarrow$ $Pr_2Fe_{14}B$ + [Fe_3B + $Pr_2Fe_{23}B_3$] $\rightarrow$ α − Fe + $Pr_2Fe_{14}B$[Fe_3B + $Pr_2Fe_{14}B$] $\rightarrow$ $PrFe_4B_4$ + [Fe_3B + $Pr_2Fe_{14}B$ + α − Fe].[17] The phases in the brackets shows those formed at the prior stage of annealing. The magnetic properties of these nanocomposites vary sensitively with the structural change during isothermal annealing. Although the effects of fine structures on the magnetic properties have been studied extensively, the phases formed in the intermediate and the final stages of annealing have not been fully understood. The ambiguities in the determination of phases arise from the facts that various phases with similar crystal structures precipitate in the annealing processes and that the previous studies have been mostly focused on the initial stage of annealing.

In the present study, therefore, the phases formed in various decomposition stages and the effects of them on the magnetic properties have been investigated by using a high-resolution electron microscopy (HRTEM).

2. Experimental Procedures

The $Pr_{4.5}$–Fe_{77}–$B_{18.5}$ amorphous ribbons were prepared by means of melt-spinning technique under argon atmosphere on a copper wheel rotating at 20 ms^{-1}. The amorphous ribbons with 30 to 50 µm thick and about 1 mm wide were obtained. The ribbons for vibrating sample magnetometer (VSM), X-ray diffraction (XRD) and HRTEM observations were encapsulated in evacuated quartz tubes prior to the isothermal heat treatments in order to prevent oxidization, and were annealed in a lead bath kept isothermally at temperatures between 650 and 760°C. The specimens were then quenched into water without breaking the capsules to suppress further reactions.

The identification of phases was carried out by XRD using a Cu-Kα_1 radiation, the selected area electron diffraction patterns obtained by TEM and the Fourier transformed patterns (FTPs) of HRTEM images. The magnetic properties of ribbons were examined at room temperature by VSM with magnetic fields up to 1.2 T. The saturation of the magnetization below 1.2 T in this alloy was confirmed by applying the magnetic field of 1.8 T. The magnetic properties were presented without demagnetization field correction. Thin foils for TEM were prepared by a conventional twinjet polishing method in the electrolyte consisting of 15% perchloric acid and 85% ethanol at −50°C and were examined in a JEOL 3010 HRTEM operating at 300 kV.

3. Results

3.1 Magnetic Properties

The variations of magnetic properties with annealing time at temperatures between 650 and 760°C are shown in Fig. 1. The effect of annealing condition on coercive force (H_c) is shown in Fig. 1(a). Annealing at 650°C induced sharp in-

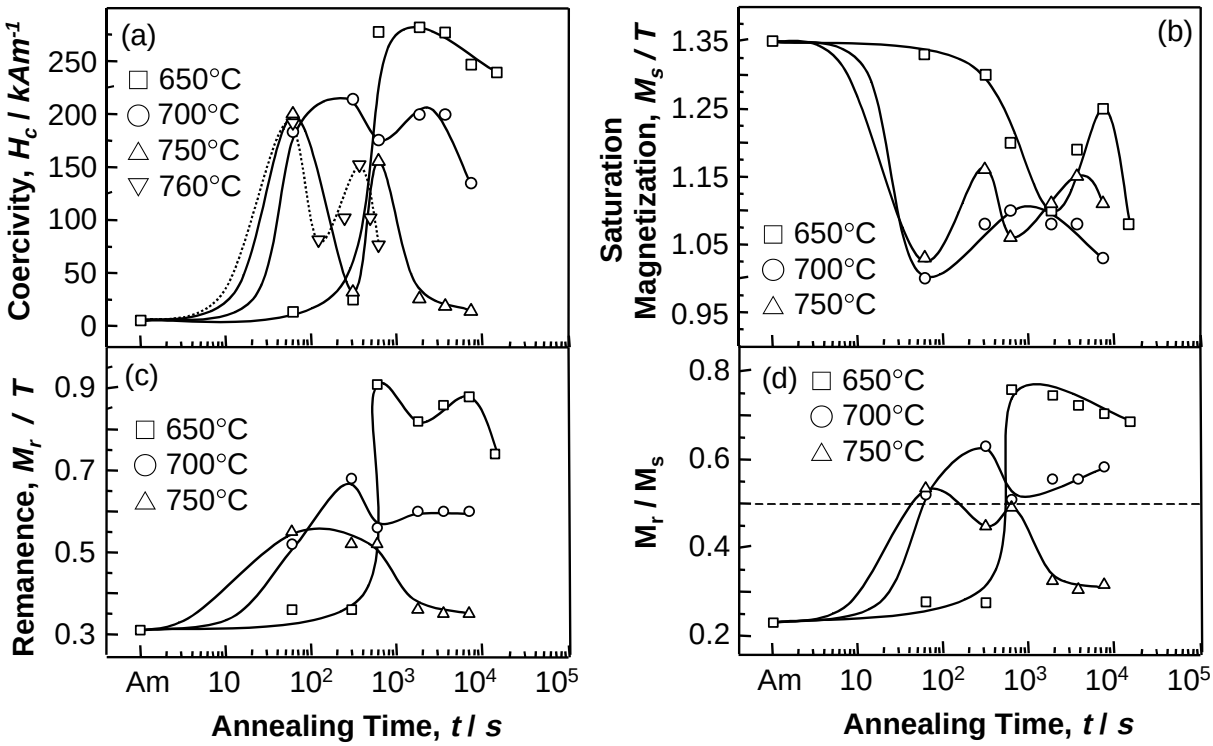

Fig. 1 Variations of magnetic properties with annealing time for $Pr_{4.5}Fe_{77}B_{18.5}$ melt-spun ribbons annealed at temperatures between 650 and 760°C. (a) the coercive force, (b) the saturation magnetization, (c) the remanence, and (d) the ratio of M_r/M_s.

crease of H_c at 10 min and decreased gradually after reaching the peak value. The variation of H_c values with annealing time at temperatures above 700°C was quite different from that at 650°C, *i.e.*, H_c increased to the first peak, decreased suddenly, increased again to the second peak and decreased gradually with annealing time. With raising annealing temperature, the first and the second peaks in H_c curves were clearly separated and were shifted to shorter time.

The saturation magnetizations (M_s) of all the annealed ribbons were smaller than that of the melt-quenched amorphous ribbon and varied in a complicated manner with annealing time as in the case of H_c (Fig. 1(b)). The M_s varied roughly in the opposite direction to that of H_c. With increasing annealing time, the M_s decreased sharply to the first minimum corresponding to the first H_c peak, increased to the first maximum peak with the decrease of H_c and decreased again to the second minimum at the second H_c peak. The remanence magnetization (M_r) varied almost in the same manner as H_c, and the maximum value of $M_r = 0.9$ T was obtained by annealing at 650°C for 10 min (Fig. 1(c)). As shown in Fig. 1(d), the M_r/M_s ratios were varied sensitively with annealing time. Since the exchange-coupling interaction between hard and soft magnetic particles can be expected in the case of $M_r/M_s > 0.5$, the exchange-coupling interaction may be small in the initial and the over-aged stages of annealing especially at 750°C, and also in the ribbons annealed for the time between the first and the second H_c peaks.

3.2 Reaction processes

Since the X-ray results at various temperatures were shown in the previous study,[17] only those for the ribbons annealed at 750°C are illustrated in Fig. 2. As reported in the previous paper,[17] the reaction processes of the $Pr_{4.5}Fe_{77}B_{18.5}$ amorphous ribbon during isothermal annealing were; Am $\rightarrow$ Fe_3B + [Am] $\rightarrow$ $Pr_2Fe_{23}B_3$ + [Am + Fe_3B] $\rightarrow$ $Pr_2Fe_{14}B$ + [Fe_3B + $Pr_2Fe_{23}B_3$] $\rightarrow$ α − Fe + $Pr_2Fe_{14}B$[Fe_3B + $Pr_2Fe_{14}B$] $\rightarrow$ $PrFe_4B_4$ + [Fe_3B + $Pr_2Fe_{14}B$ + α − Fe]. After the crystallizations of amorphous phase into Fe_3B, $Pr_2Fe_{23}B_3$ and $Pr_2Fe_{14}B$, the diffraction peaks from $Pr_2Fe_{23}B_3$ disappeared but the intensity of the reflections from α-Fe increased with annealing time (Figs. 2(b) and (c)). The disappearance of $Pr_2Fe_{23}B_3$ was accelerated with increasing temperature. In the final stages of annealing, the intensity of Fe_3B reflection decreased, but those of both α-Fe and $PrFe_4B_4$ increased (Figs. 2(c) and (d)).

3.3 Nanostructures

Figure 3 shows the HRTEM image at the early stage of crystallization at 650°C for 1 min. In this figure, (b) to (d) are the FTPs for the particles marked "b", "c" and "d" within (a), and (e) to (g) are the schematic illustrations for (b) to (d), respectively. Three fine particles with about 20 nm diameter were observed and were inter-linked with neighboring particles. The three particles "b", "c" and "d" were confirmed to be soft magnetic Fe_3B, $Pr_2Fe_{23}B_3$, and Fe_3B particles, respectively, and the interfaces between them were almost continuous.[17] In the FTP shown in Fig. 3(c), the reflections from a $Pr_2Fe_{23}B_3$ particle were shown by white squares to discriminate them from the reflections due to the particles in the vicinity of the $Pr_2Fe_{23}B_3$.

The HRTEM image for the ribbon annealed at 650°C for 5 min where H_c begins to increase is shown in Fig. 4. A hard

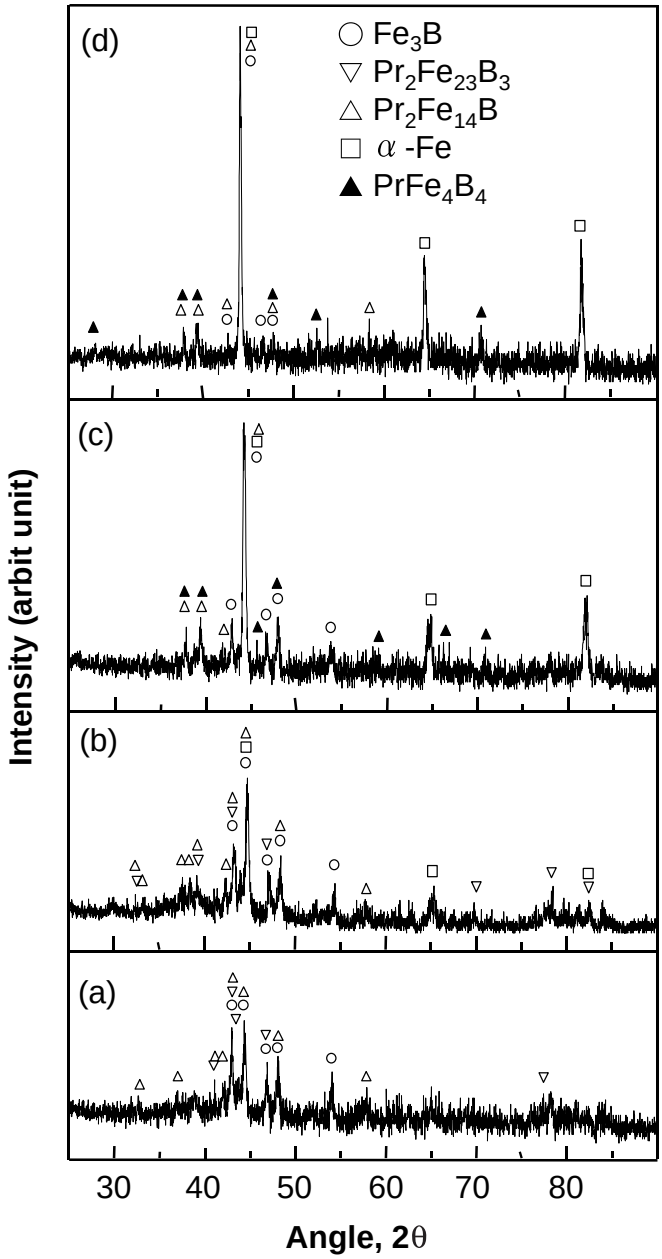

Fig. 2 XRD patterns for melt-spun $Pr_{4.5}Fe_{77}B_{18.5}$ ribbons annealed at 750°C. (a) 1 min, (b) 10 min, (c) 30 min, and (d) 2 h.

magnetic $Pr_2Fe_{14}B$ particle "b" nucleated contact with a Fe_3B particle "c". Another $Pr_2Fe_{14}B$ particle "d" formed near the $Pr_2Fe_{23}B_3$ particle "e". The interphase boundaries among the particles were continuous as far as two-dimensional observation.[17] With increasing annealing time, the amounts of both $Pr_2Fe_{14}B$ and Fe_3B particles increased as shown in Fig. 5 and the particles were coalesced by further annealing.

Typical TEM and HRTEM micrographs for the ribbon annealed at 750°C for 10 min are shown in Fig. 6. The heat treatment was carried out in the condition where the second H_c peak was observed in Fig. 1. The ribbon is consisted of relatively coarse grains with diameter ranging from 30 to 60 nm involving large amounts of extremely fine particles less than 5 nm. The grains involving the fine particles were confirmed as $Pr_2Fe_{14}B$ and the fine particles distributed within them were identified as α-Fe by the analysis of the FTPs shown in Figs. 6(c) to (f). The fine α-Fe particles distributed homogeneously within a $Pr_2Fe_{14}B$ particle as if they were formed by a eutectoid decomposition from $Pr_2Fe_{23}B_3$. These α-Fe particles grew by further annealing.

Figure 7 shows the micrographs for the ribbon annealed at 700°C for 30 min, corresponding to almost the final stage of annealing. A large particle, marked "c", was enclosed by the particle "d" as shown in Fig. 7(a). The HRTEM images for the particles "c" and "d" are presented in Fig. 7(b). The particles marked "c" and "d" in Fig. 7(b) were $PrFe_4B_4$ and $Pr_2Fe_{14}B$, respectively.

4. Discussion

The $Pr_{4.5}Fe_{77}B_{18.5}$ amorphous ribbon decomposes in the following sequence; Am $\rightarrow$ Fe_3B + [Am] $\rightarrow$ $Pr_2Fe_{23}B_3$ + [Am + Fe_3B] $\rightarrow$ $Pr_2Fe_{14}B$ + [Fe_3B + $Pr_2Fe_{23}B_3$] $\rightarrow$ α-Fe + $Pr_2Fe_{14}B$[Fe_3B+$Pr_2Fe_{14}B$] $\rightarrow$ $PrFe_4B_4$+[Fe_3B+$Pr_2Fe_{14}B$+ α-Fe].[17] The variation of magnetic properties of the ribbon will be discussed in relation to this microstructural change.

Figure 8 is a schematic illustration for the variations of H_c and M_s with isothermal annealing time. In the range from A to B, the magnetic properties of ribbons annealed at 650°C to 1 min are almost the same as those of the melt-quenched amorphous ribbon as can be seen in Fig. 1. The ribbon at this stage of annealing, however, is consisted of soft magnetic particles such as Fe_3B and $Pr_2Fe_{23}B_3$ as shown in Fig. 3. After some incubation time, H_c increases and M_s decreases sharply in the range from B to C. At this stage, hard magnetic $Pr_2Fe_{14}B$ particles forms continuously on the interfaces of Fe_3B or $Pr_2Fe_{23}B_3$ particles[17] and the amount of $Pr_2Fe_{14}B$ particles increases with annealing time as shown in Figs. 4 and 5. Thus, the high H_c value is due to the formation of $Pr_2Fe_{14}B$ particles.

The existence of the exchange-coupling interaction between hard magnetic $Pr_2Fe_{14}B$ and soft magnetic Fe_3B (or $Pr_2Fe_{23}B_3$) particles can be recognized from the high M_r/M_s ratios > 0.5 as shown in Fig. 1(d). It should be noted that M_s decreases drastically with the formation of the $Pr_2Fe_{14}B$ particles. In the range from C to D, H_c decreases abruptly but M_s increases. At this stage of annealing, the crystallized Fe_3B, $Pr_2Fe_{23}B_3$ and $Pr_2Fe_{14}B$ particles grow and coalesce. Thus the exchange-coupling interaction inducing high H_c is reduced. The M_s, however, increases due to the increase of soft magnetic particles as shown in Fig. 1(d).

In the range from D to E, H_c increases again with the decrease of M_s. At this stage of annealing, new $Pr_2Fe_{14}B$ particles involving very fine α-Fe particles precipitate. These particles form probably by the eutectoid-like decomposition of metastable $Pr_2Fe_{23}B_3$ particles. The results showing high H_c values again are mainly originated from increasing of the volume fraction of $Pr_2Fe_{14}B$ particles and partly from the strong exchange-coupling interactions between $Pr_2Fe_{14}B$ and α-Fe particles within them.

The fact that the precipitation of α-Fe particles increases the H_c value is consistent with those reported by Inoue *et al.*[15,16] where the $Nd_7Fe_{90-88}B_{3-5}$ alloys comprising amorphous phase, α-Fe, and hard magnetic particles exhibit high H_c values. They also suggested that α-Fe particles play an

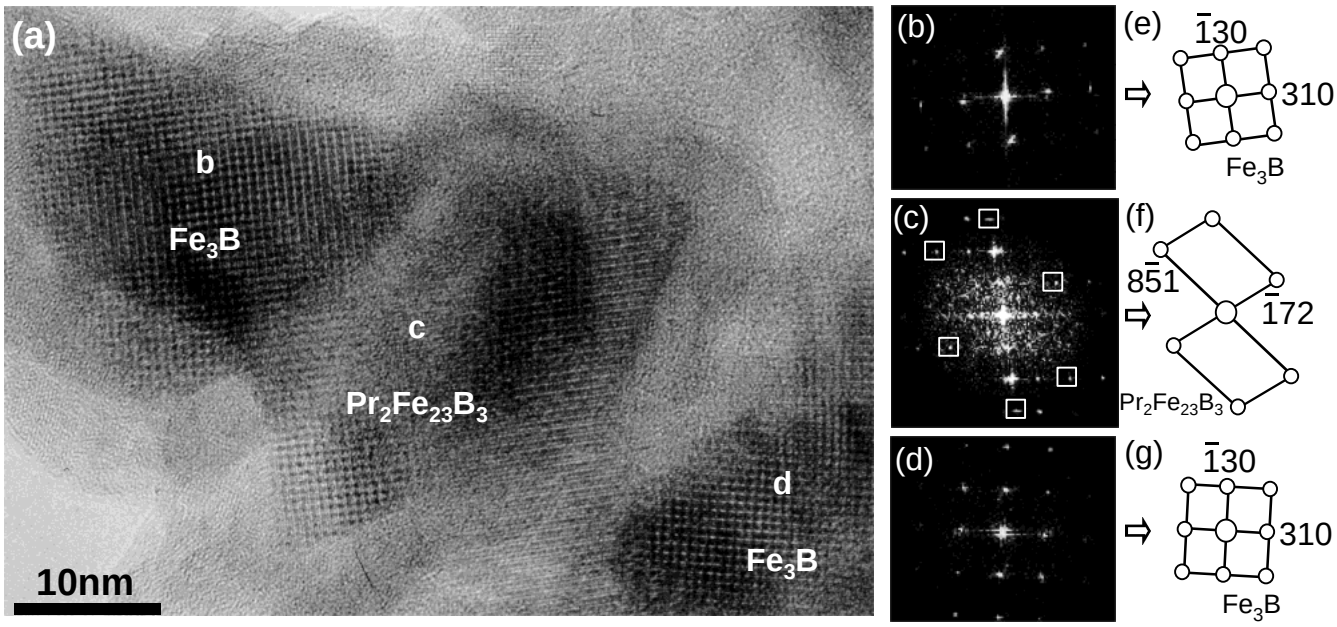

Fig. 3 HRTEM micrograph for melt-spun $Pr_{4.5}Fe_{77}B_{18.5}$ ribbon annealed at 650°C for 1 min. (a) HRTEM image, (b) to (d) the Fourier transformed patterns for the particles marked "b", "c" and "d" within (a), respectively, and (e) to (g) the schematic illustrations for (b) to (d), respectively.

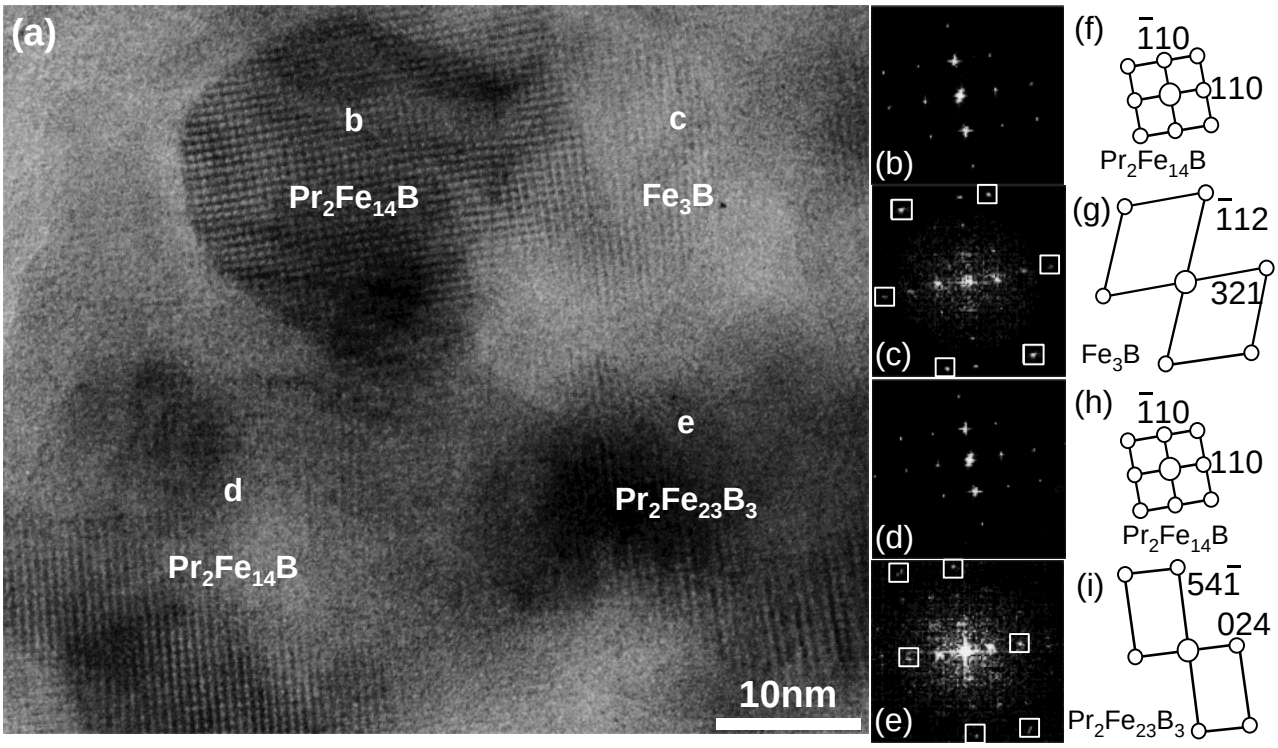

Fig. 4 HRTEM micrograph for melt-spun $Pr_{4.5}Fe_{77}B_{18.5}$ ribbon annealed at 650°C for 5 min. (a) HRTEM image, (b) to (e) the Fourier transformed patterns for the particles marked "b", "c", "d" and "e" within (a), respectively, and (f) to (i) the schematic illustrations for (b) to (e), respectively.

important role in obtaining the good magnetic properties.[15,16] Although the formation of α-Fe particles are very important for obtaining high H_c and M_s simultaneously, H_c decreases when the α-Fe particles grow larger than 5 nm in diameter.

In the final stages, *i.e.*, in the range from E to F, both H_c and M_s decreases gradually with increasing annealing time. At this stage, the $PrFe_4B_4$ enclosing α-Fe grains forms.[17] If $Pr_2Fe_{14}B$ decomposes into both $PrFe_4B_4$ and α-Fe, H_c will decrease drastically almost the same level to the as-melt-quenched amorphous ribbon, and the M_s will be reduced as can be seen in Fig. 1.

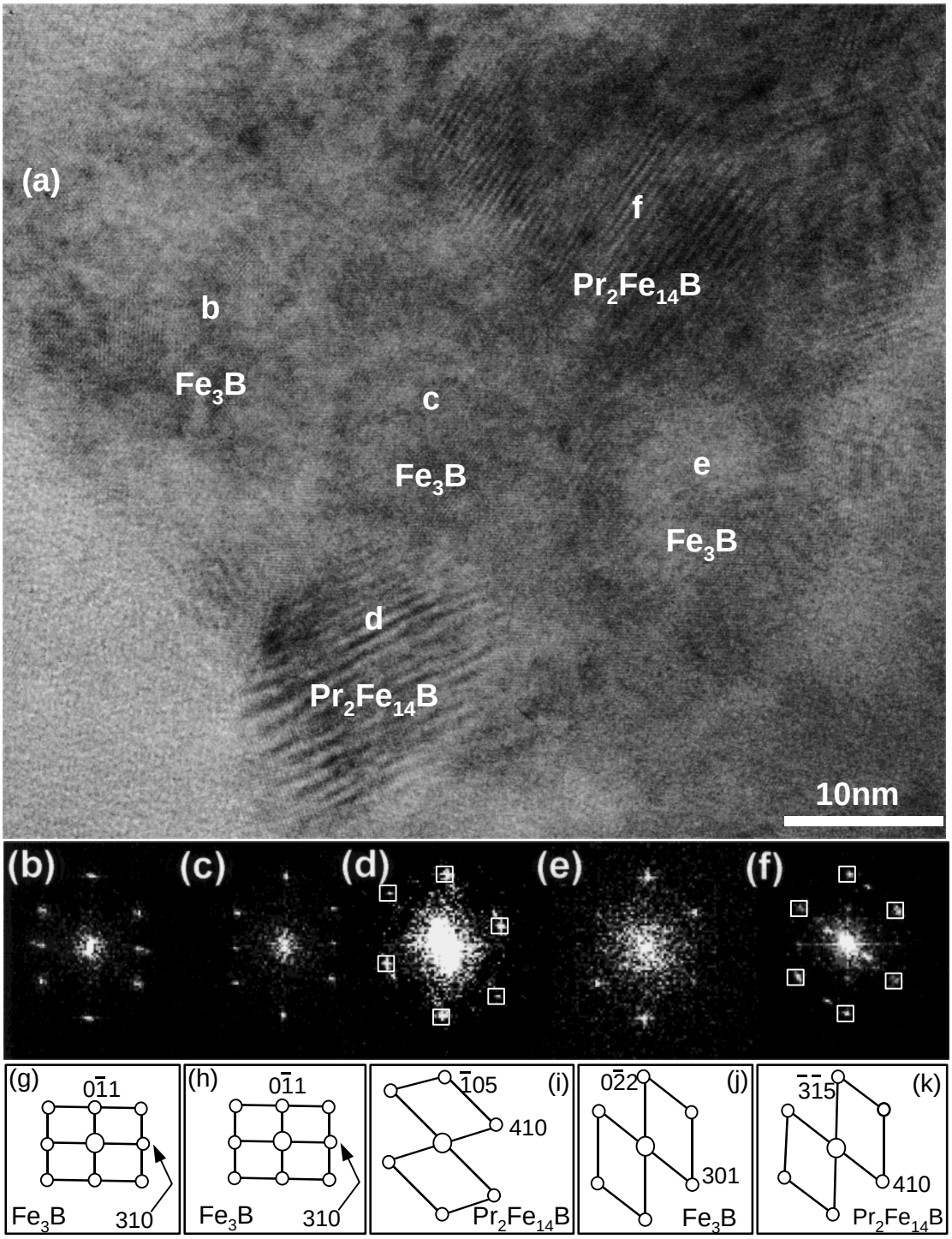

Fig. 5 HRTEM micrograph for melt-spun $Pr_{4.5}Fe_{77}B_{18.5}$ ribbon annealed at 650°C for 10 min. (a) HRTEM image, (b) to (f) the Fourier transformed patterns for the particles marked "b", "c", "d", "e" and "f" within (a), respectively, and (g) to (k) the schematic illustrations for (b) to (e), respectively.

5. Conclusions

(1) The two separate reactions inducing high H_c values can be observed during the isothermal annealing of $Pr_{4.5}Fe_{77}B_{18.5}$ amorphous ribbons.

(2) The first high H_c peak arises from the precipitation of $Pr_2Fe_{14}B$ particles after the formation of soft magnetic Fe_3B and $Pr_2Fe_{23}B_3$ particles. At this annealing stage, H_c increases but M_s decreases significantly with isothermal annealing time.

(3) The second H_c peak, which was been newly observed in the present study, is due to a eutectoid-like decomposition of $Pr_2Fe_{23}B_3$ particles into $Pr_2Fe_{14}B$ and α-Fe particles within them. The mechanism inducing high H_c values is due to the increase in the volume fraction of $Pr_2Fe_{14}B$ particles as well as the exchange-coupling interaction between $Pr_2Fe_{14}B$ and α-Fe particles.

(4) The decomposition of $Pr_2Fe_{14}B$ into $PrFe_4B_4$ and the

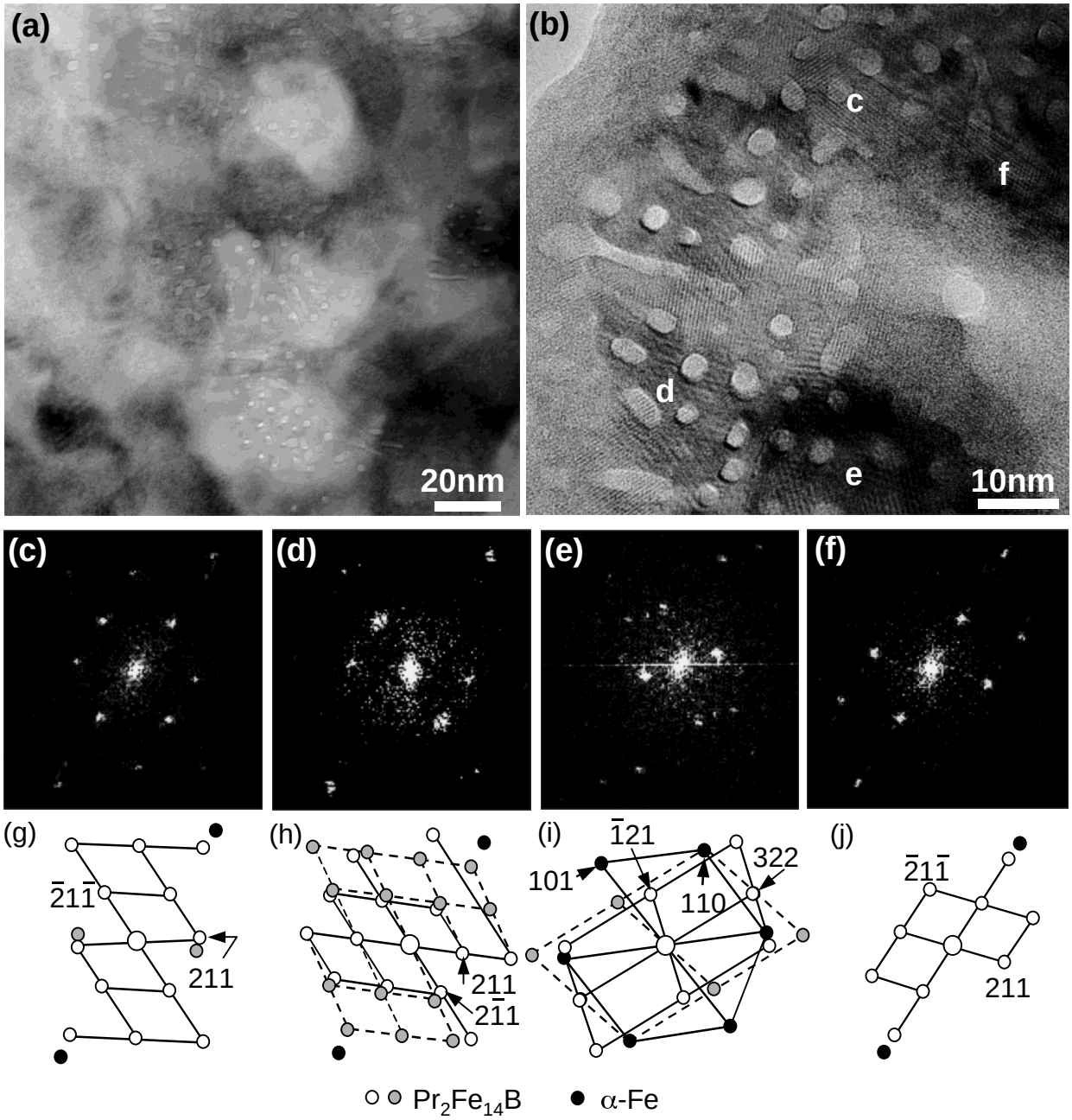

Fig. 6 Micrographs for melt-spun $Pr_{4.5}Fe_{77}B_{18.5}$ ribbon annealed at 750°C for 10 min. (a) conventional TEM image, (b) HRTEM image taken from a grain within (a), (c) to (f) the Fourier transformed patterns from the regions marked "c", "d", "e", and "f" within (b), respectively, and (g) to (j) the schematic illustrations for (c) to (f), respectively.

coarsening of these particles reduce the magnetic properties of the ribbons.

Acknowledgements

This study was partially supported by The Japan Society for the Promotion of Science. Y.-C. J. would like to express his sincere gratitude to JSPS.

REFERENCES

1) E. F. Kneller and R. Hawig: IEEE Trans. Magn. **27** (1991) 3588–3600.
2) L. Withanawasam and G. C. Hadjipanyis: J. Appl. Phys. **76** (1994) 7065–7077.
3) S. Hirosawa and H. Kanekiyo: Mater. Sci. and Eng. **A217/218** (1996) 367–370.
4) L. H. Lewis, K. Gallagher, B. Hoerman and V. Panchanathan: J. Alloys Comp. **270** (1998) 265–274.
5) M. V. P. Altoé, M. S. Lancarotte, H. R. Rechenberg and F. P. Missell: IEEE Trans. on Magn. **31** (1995) 3614–3616.
6) M. Uehara, S. Hirosawa, H. Kanekiyo, N. Sano and T. Tomida: NanoStructured Mater. **10** (1998) 151–160.
7) F. Matsumoto, H. Sakamoto, M. Komiya and M. Fujikura: J. Appl. Phys. **63** (1988) 3507–3509.
8) H. Kanekiyo and S. Hirosawa: J. Mag. Soc. Jpn., **17** (1993) 185–190.
9) R. Coehoorn, D. B. de Mooij, J. P. W. B. Duchateau and K. H. J. Buschow: J. de Phys. **49** (1988) C8–669–670.
10) K. H. J. Buschow, D. B. de Mooij and R. Coehoorn: J. Less-Common Met. **145** (1988) 601–611.
11) S. Hirosawa, H. Kanekiyo and M. Uehara: J. Appl. Phys., **73** (1993) 6488–6490.

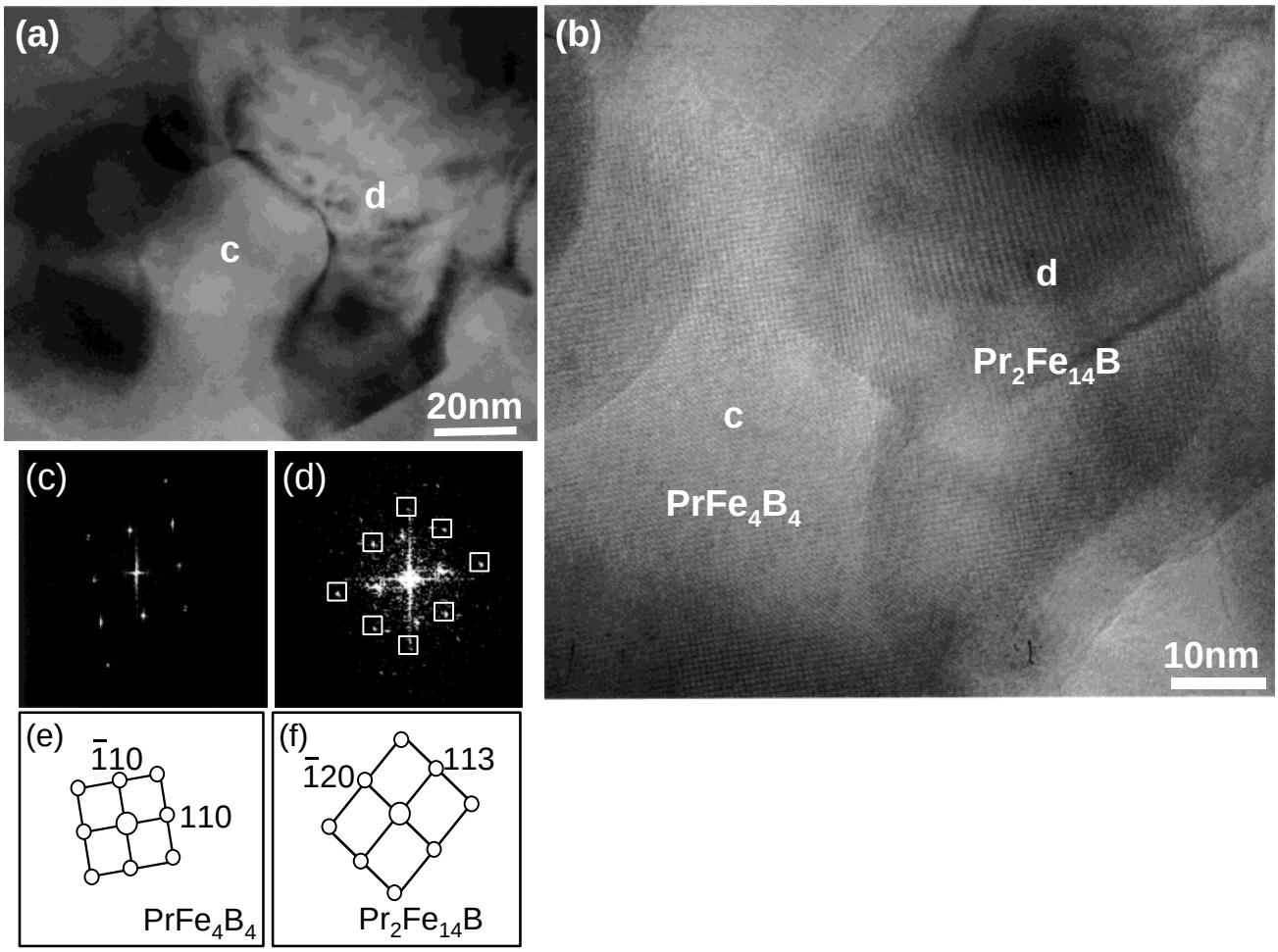

Fig. 7 Micrographs for melt-spun $Pr_{4.5}Fe_{77}B_{18.5}$ ribbon annealed at 750°C for 30 min. (a) typical TEM image, (b) HRTEM image for (a), (c) and (d) the Fourier transformed patterns for the particles marked "c" and "d" within (a), respectively, and (e) and (f) the schematic illustrations for (c) and (d), respectively.

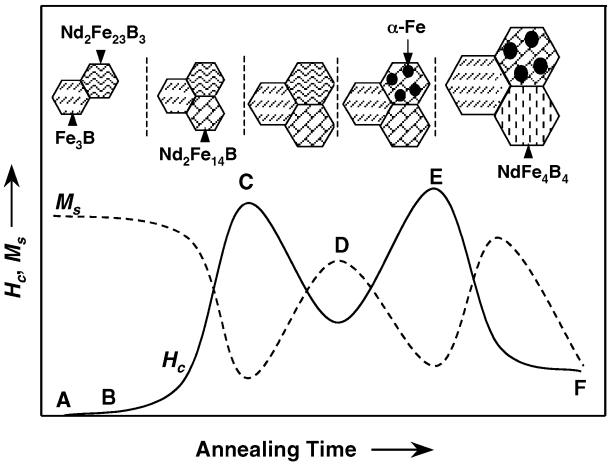

Fig. 8 The schematic illustration of the relationships between coercive force, saturation magnetization, nanostructures and isothermal annealing time.

12) S. Hirosawa and H. Kanekiyo: Mater. Sci. Eng. **A217/218** (1996) 367–370.
13) B. X. Gu, B. G. Shen and R. H. Zhai: J. Magn. Magn. Mater. **124** (1993) 85–88.
14) T. Hinomura, S. Nasu, H. Kanekiyo, M. Uehara and S. Hirosawa: Mater. Trans., JIM **38** (1997) 1106–1115.
15) A. Inoue, A. Takeuchi, A. Makino and T. Masumoto: Mater. Trans., JIM **36** (1995) 676–685.
16) A. Inoue, A. Takeuchi, A. Makino and T. Masumoto: Mater. Trans., JIM **36** (1995) 962–971.
17) Y.-C. Jung, Y. Ohmori, K. Nakai, S. Hirosawa and H. Kanekiyo: Mater. Trans. **42** (2001) 2102–2111.